ISSN (Print) 1226-1750
ISSN (Online) 2233-6656
Journal of Magnetics 31(2), 125-135 (2026) https://doi.org/10.4283/JMAG.2026.31.2.125

Study on the Magnetic and Mechanical Properties of Dy-diffused Nd-Dy-Fe-B Magnets

Weiyuan Zhang[1], Xianghao Zhang[1], Long Wang[2], Fan Yang[1], Yilong Ma[3], Zhihua Hu[1]*, and Tianguo Wang[1]*

[1]*School of Automotive Materials, Hubei University of Automotive Technology, Shiyan 442002, China*
[2]*State Key Laboratory of Refractory Materials and Metallurgy, Wuhan University of Science and Technology, Wuhan 430081, China*
[3]*School of Metallurgy and Power Engineering, Chongqing University of Science and Technology, Chongqing 401331, China*

(Received 22 February 2026, Received in final form 10 April 2026, Accepted 13 April 2026)

Understanding the synergistic mechanism of the Dy element in grain-boundary-diffused Nd-Fe-B magnets is important for enhancing the performance of these magnets. In this paper, the magnetic and mechanical properties of Dy-diffused Nd-Dy-Fe-B magnets were investigated. Results showed that Dy in the matrix increased the H_{cj} of the matrix, but reduced the ΔH_{cj} of diffused magnets. The fracture toughness of the matrices decreased with increasing Dy content. Still, it was higher than that of corresponding diffused magnets, indicating that Dy grain boundary diffusion reduced the fracture toughness of Nd-Dy-Fe-B magnets. The increase in Dy content in matrices led to the formation of core-shell structure (Dy-rich core and Dy-lean shell) grains, resulting in a decrease in the utilization efficiency of the Dy element during the grain boundary diffusion process (GBDP). These results demonstrated the synergistic effect of Dy, providing a theoretical basis for reducing its content in diffused magnets.

Keywords : grain boundary diffusion, mechanical properties, Nd-Dy-Fe-B magnets

1. Introduction

Sintered Nd-Dy-Fe-B magnets are widely used to manufacture various kinds of electric-driven motors due to their excellent magnetic properties and higher operating temperatures [1]. Meanwhile, with the rapid development of the electric vehicle industries, sintered Nd-Dy-Fe-B magnets with higher operating temperatures and lower cost are required to enhance the competitiveness of Nd-Fe-B manufacturing enterprises [2, 3]. So it is an extremely significant and timely topic to fabricate more cost-effective, high-performance Nd-Fe-B magnets by more effectively utilizing the Dy element. According to previous literature [4-6], the GBDP is the most effective method to improve the intrinsic coercivity (H_{cj}) of sintered Nd-Fe-B magnets with minimal heavy rare-earth consumption. It has been well studied and rapidly industrialized. The mechanism of enhancing the H_{cj} of magnets by Dy grain boundary diffusion is that Dy grain boundary diffusion can form a Dy-rich hard magnetic shell layer, effectively inhibiting the nucleation reversal phenomenon on the surface of main phase grains under low magnetic fields, thus effectively enhancing the H_{cj} of sintered Nd-Fe-B magnets [7-10]. Till now, Pure Dy and Dy-rich compounds (DyH_x, DyF_3, Dy-Cu) have been used as diffusion sources, demonstrating different effects on improving the H_{cj} of sintered Nd-Fe-B magnets [11-14]. The H_{cj} of sintered Nd-Dy-Fe-B magnets increases linearly with Dy content at about 2.2 kOe/wt% Dy [15], and the H_{cj} of diffused Nd-Dy-Fe-B magnets with a thickness of 3 mm is 5.64 kOe and 2.63 kOe higher than that of the matrix when the diffusion weight of Dy is 0.3 wt% and 0.1 wt%, respectively [7]. However, the Dy content in the matrix can also affect Dy grain boundary diffusion, which enhances the magnetic properties of diffused magnets, and there are few research results in this area.

Sintered Nd-Fe-B magnets exhibit a multi-phase structure characterized by different grain orientations and thermal expansion coefficients, which are highly sensitive to changes in their mechanical properties [16]. Higher Nd

*Corresponding author: Tel: +86-0719-8238783
e-mail: huzhihua_1@163.com(Zhihua Hu)
e-mail: 53812938@qq.com(Tianguo Wang)

content corresponds to smaller main phase grains and a large amount of Nd rich precipitates within the fracture, thereby improving the impact fracture toughness of sintered Nd-Fe-B magnets [17]. Substituting some Nd elements with Dy elements can enhance the impact stability of sintered Nd-Fe-B magnets. Still, the strength and hardness of Nd-Fe-B magnets doped with Dy decrease due to the reduced resistance to crack propagation along grain boundaries [18-20]. The mechanical properties of sintered Nd-Dy-Fe-B magnets with different Dy content have been investigated in the previous work, and the results indicate that the mechanical properties of Nd-Fe-B magnets are highly sensitive to their microstructure [22]. In this paper, the mechanical properties of sintered Nd-Dy-Fe-B magnets with different Dy content were retested for comparison with the mechanical properties of diffused magnets to explore the influence of Dy grain boundary diffusion on the mechanical properties of diffused magnets.

2. Experimental

The original magnets with nominal compositions $(PrNd)_{31.5-x}Dy_xFe_{bal}Co_{0.2}M_{0.73}B_{0.98}$ (wt%, x=0, 1, 2, 3) were obtained by the dual-alloy powder-mixing method and denoted as Dy0, Dy1, Dy2 and Dy3, respectively. The specific experimental preparation method was described in Ref. [21], and the sintering temperature of the original magnets was 1075 ℃. The large rectangular original magnets were cut into 45 mm × 25 mm × 6 mm matrices. All of the matrices were polished with fine sandpaper before Dy grain boundary diffusion. Ethanol as a solvent mixed with Dy slurry in a ratio of 1 gram: 5 milliliters to obtain Dy diffusion dispersant, and then the Dy diffusion dispersant was uniformly coated on two planes of 45 mm × 25 mm of the matrix, with a coating amount of 0.4 wt%, calculated as the mass ratio of DyH to the matrix. The coated matrices were dried and then placed in a tube vacuum sintering furnace, followed by grain boundary diffusion treatment at 920 ℃ for 10 h and subsequently tempered at 490 ℃ for 4 h. The matrices and corresponding diffused magnets were cut into circular samples with a diameter of 10 mm, and the sample surfaces were polished to perform various experimental tests and analyses. A NIM-62000TB hysteresis loop tracer measured the magnetic properties of samples. The Vickers hardness measurements were carried out on the samples using a hardness tester. 10 indents were made on polished surfaces for each sample, with a 30 kg load held

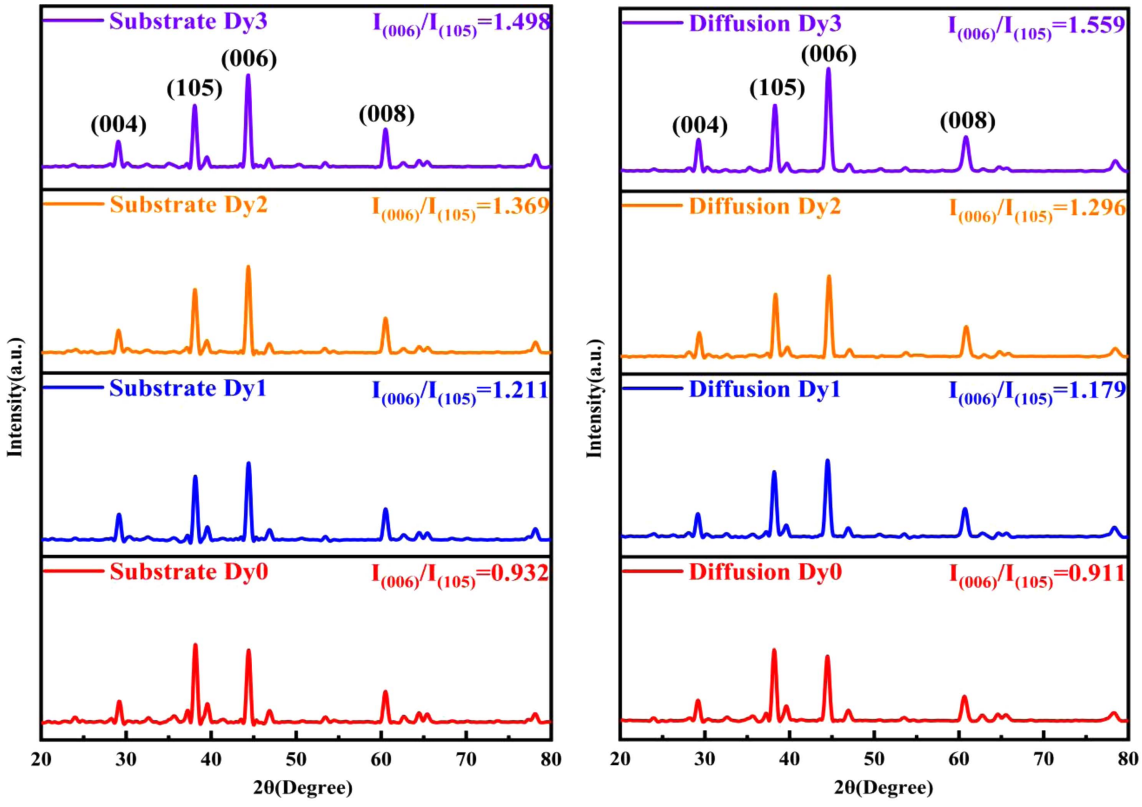

Fig. 1. (Color online) XRD patterns of the matrices and corresponding diffused magnets.

for 15 s, and the average Vickers hardness was determined. The fracture toughness (KIC) data were sourced from the experimental method described in Ref. [22], which can only be used to compare the relative rankings of mechanical properties among samples. The alignment of the sample surface perpendicular to the c-axis was examined by X-ray diffraction with Cu Kα radiation. The field emission scanning electron microscope (SEM JEOL JSM-7900F) was used to characterize the microstructure of the sample surface, and TEM images and selected-area electron diffration (SAED) patterns were obtained utilizing transmission electron microscopy (TEM, FEI Tecnai G2 F20) with energy-dispersive X-ray spectroscopy (EDS).

3. Results and Discussion

XRD patterns of matrices and corresponding diffused magnets are shown in Fig. 1. It can be seen that the intensity of the (006) diffraction peak is lower than that of the (105) diffraction peak only for the matrix without Dy content and corresponding diffused magnets. The orientation degree of sintered Nd-Fe-B magnets can be qualitatively described by the intensity ratio of (006) and (105) diffraction peaks. The intensity ratio of the (006) and (105) diffraction peaks on matrices and corresponding diffused magnets increases with increasing Dy content in the matrix, indicating that Dy can improve the orientation of sintered Nd-Fe-B magnets prepared by the dual alloy powder mixing method.

The magnetic properties and squareness factor (SF) of matrices and corresponding diffused magnets are shown in Fig. 2. The H_{cj} of matrices and corresponding diffused magnets increases with increasing Dy content in the matrix, indicating that Dy grain boundary diffusion does not change the variation trend of H_{cj}. The H_{cj} increment (ΔH_{cj}) after Dy grain boundary diffusion first declines, and then increases with increasing Dy content in the matrix. When the Dy content of the matrix is 0, the ΔH_{cj} of the corresponding diffused magnet is the largest, with a maximum value of 3.88 kOe, resulting in the H_{cj} of the diffused magnet being equal to that of the Dy2 matrix. The trend in the squareness factor (SF) of diffused magnets is consistent with that of $(BH)_{max}$ as the Dy content in the matrix increases.

The remanence (B_r) of matrices and corresponding diffused magnets declines with increasing Dy content in the matrix because the saturation magnetization J_s (7.1 kGs) of $Dy_2Fe_{14}B$ is far less than that of $Nd_2Fe_{14}B$ [23]. Simultaneously, the B_r of matrices is higher than that of corresponding diffused magnets because Dy grain boundary diffusion either reduces the proportion of the main phase or decreases the saturation magnetization J_s of the main

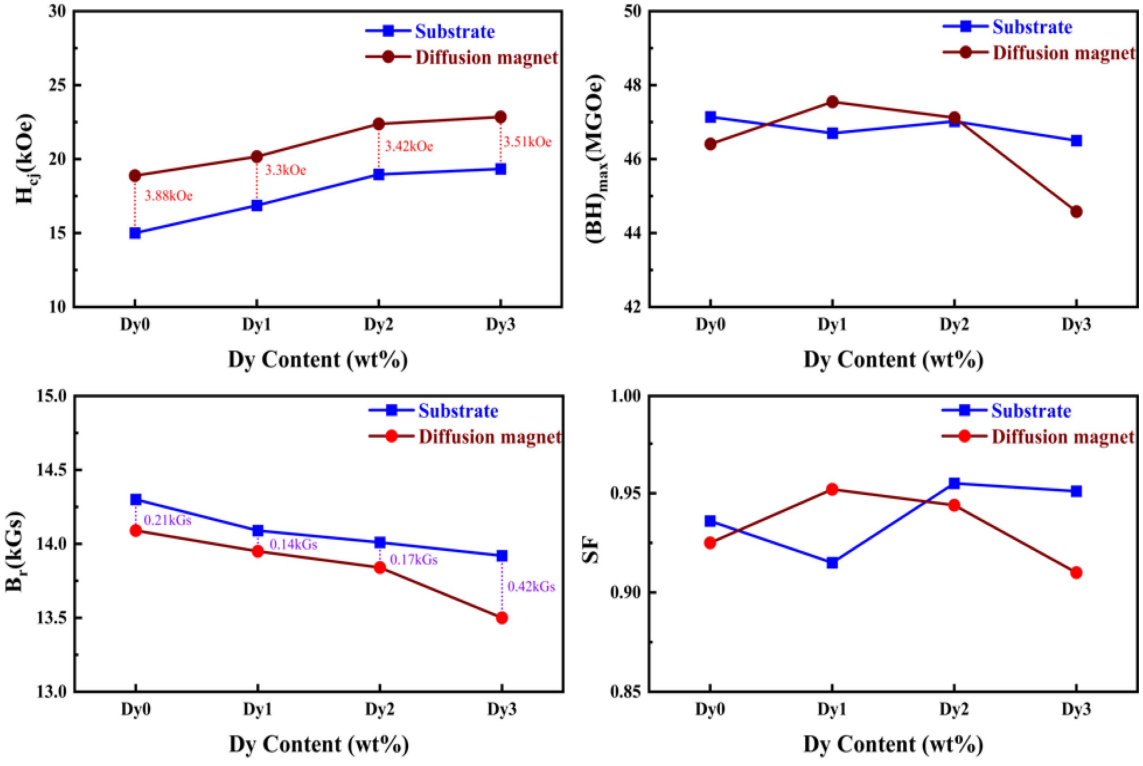

Fig. 2. (Color online) Magnetic properties and SF of matrices and corresponding diffused magnets.

phase. The B_r and $(BH)_{max}$ of diffused magnets decrease more significantly than those of the matrix when the Dy content in the matrix increases from 2.0 wt % to 3.0 wt %. When the Dy content of the matrix is 3.0 wt %, the decrease in B_r of the corresponding diffused magnet is the largest, with a maximum reduction of 0.42 kGs, as indicated by the change in orientation degree in Fig. 1 and the following formula [24].

$$B_r = A \cdot J_s \cdot (\rho/\rho_0) \cdot (1-\alpha) \cdot f \quad (1)$$

where A is the volume fraction of positive magnetic domains, J_s is saturation magnetization, ρ/ρ_0 is relative density, α is volume fraction of nonmagnetic phase, and f is degree of alignment. The reason for the sharp decrease in the B_r of the Dy3 matrix after Dy grain boundary diffusion should be the significant decrease in the volume fraction of positive magnetic domains, and Dy grain boundary diffusion deteriorates the microstructure of the corresponding diffused magnet.

Fig. 3 presents BSE-SEM images of the matrices and the corresponding diffused magnets. The Dy-rich shell of (Dy, $NdPr)_2Fe_{14}B$ phase is observed, and a large amount of core-shell structure grains with $(NdPr)_2Fe_{14}B$ (core)/(Dy, $NdPr)_2Fe_{14}B$ (shell) in Fig. 3(A). The basic coercivity mechanism of sintered Nd-Fe-B magnets is generally accepted as demagnetization domain nucleation, and the magnetization reversal in sintered Nd-Fe-B magnets preferentially occurs at the edges of the main phase grains and then rapidly propagates to the whole magnet [25, 26]. Optimizing the GB and the interface between the GB phase and the main phase can effectively prevent magnetization reversal from propagating in a cascade

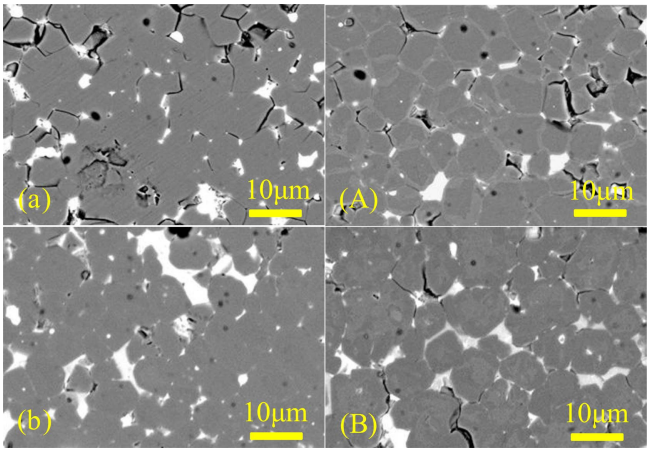

Fig. 3. (Color online) BSE SEM images of the matrices (a-Dy0 and b-Dy2) and corresponding diffused magnets (A-Dy0 and B-Dy2).

throughout the entire magnet, thereby increasing the intrinsic coercivity [27]. During the GBDP, Dy atoms can diffuse into the magnet through the liquid Nd-rich GB phase. Nd atoms are substituted by Dy atoms in the surface layer of the main phase to form a Dy-rich shell of (Dy, $Nd)_2Fe_{14}B$ phase, which can optimize the GB and the interface between the GB phase and the main phase, leading to obviously increase the intrinsic coercivity of diffused magnets [28]. As for the Dy0 matrix, the Hcj of the corresponding diffused magnets is higher than that of the matrix.

A large amount of Dy is distributed on the grain surfaces, forming a Dy-rich core in Fig. 3(B). The phenomenon leads to the formation of a large number of core-shell grains with (Dy, $NdPr)_2Fe_{14}B$ (Dy-rich core)/(Dy, $NdPr)_2Fe_{14}B$ (Dy-lean shell). The atomic radius of Nd is about 5 % larger than that of Dy, and the covalent radius of Nd is about 3 % larger than that of Dy [29]. If the atomic radius of the diffusion source (heavy rare earths and their hydrides) is smaller than that of Nd in Nd-Fe-B magnets, its diffusion mechanism includes not only grain boundary diffusion but also lattice diffusion [30]. But in the high-Dy level regime, the Dy concentrations of the reprecipitated $Re_2Fe_{14}B$ phases are still increased and reach a similar Dy/RE ratio value as that of solid-state-diffused (Dy, $NdPr)_2Fe_{14}B$ grains due to a high diffusion rate, which leads to diminishing the grains with the Dy-lean core/Dy-rich shell microstructure [31]. Although the ΔH_{cj} of diffused magnets is attributed to the joint contribution of these two diffusion mechanisms (grain boundary diffusion and lattice diffusion), the ΔH_{cj} by grain boundary diffusion is higher than that by lattice diffusion [11]. So the presence of Dy in the matrix reduces the effect of Dy grain-boundary diffusion on improving the intrinsic coercivity of the diffused magnet.

The content of Nd and Pr elements in the white Nd-rich phase is higher than that in the main phase grains, while the content of Dy element in the white Nd-rich phase is lower than that in the main phase grains. Two types of shell structures and the distribution of rare-earth elements in the surface morphology of diffused magnets can be distinguished in the elemental mapping images in Fig. 4, but their resolution is much lower than that observed with an electron probe microanalyzer (EPMA) [5]. The composition of the main phase grains and white particles in Fig. 4 is shown in Table 1. Al element tends to be uniformly distributed along grain boundaries, and Al-containing low-melting phases are formed in the intergranular phase, improving the wettability between the main phase and the grain boundary phase [32, 33]. Al element is detected in the main phase grains, with a slight

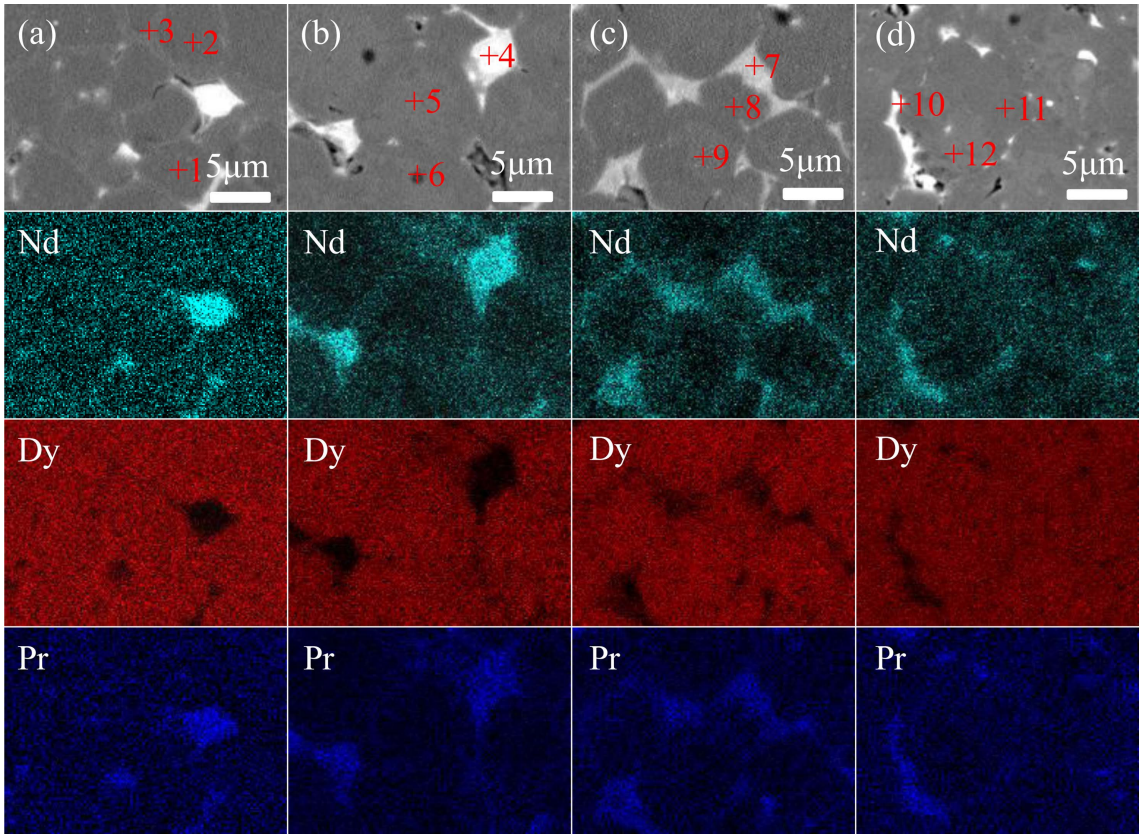

Fig. 4. (Color online) SEM images and element mapping images on the surface of diffused magnets: a-Dy0, b-Dy1, c-Dy2 and d-Dy3.

Table 1. Composition of the main phase grains and white Nd-rich phase particles in Fig. 4.

Dy content (wt %)	Position	Composition (wt %)							
		Nd	Pr	Dy	Fe	Al	Cu	O	Zr
0	1	20.84	6.12	0.45	70.74	1.86	0	0	0
	2	20.92	6.34	1.05	69.77	1.91	0	0	0
	3	19.96	5.86	2.65	69.7	1.84	0	0	0
1	4	36.49	16.99	2.69	37.07	2.06	0	4.71	0
	5	10.15	2.82	16.21	69.01	1.8	0	0	0
	6	16.6	4.79	6.58	70.24	1.79	0	0	0
2	7	36.88	15.92	1.94	35.67	3.51	1.15	1.49	3.43
	8	15.41	4.76	8.24	69.61	1.96	0	0	0
	9	8.83	2.35	17.91	69.12	1.79	0	0	0
3	10	38.56	17.01	4.31	31.4	2.7	4.37	1.65	0
	11	9.13	2.75	17.74	68.65	1.73	0	0	0
	12	13.88	3.99	10.47	69.75	1.9	0	0	0

difference in Al content, resulting in a decrease in the B_r of sintered Nd-Dy-Fe-B magnets. Al, Cu, and Zr elements are detected in white Nd-rich phase particles, but there are also some white Nd-rich phase particles where Cu and Zr elements are not detected. The H_{cj} of sintered Nd-Dy-Fe-B magnets can be enhanced by adding Al, Cu, or Zr [34-36].

As for the matrix containing Dy, there are two types of grain composition for the corresponding diffused magnets. One is the main-phase grain with Dy content

higher than NdPr content, forming core-shell grains with (Dy, NdPr)$_2$Fe$_{14}$B (Dy-rich core)/(Dy, NdPr)$_2$Fe$_{14}$B (Dy-lean shell). The other is the main-phase grain with Dy content lower than NdPr content, and the difference in Dy content between the two components is obvious. Meanwhile, the Dy content in white Nd-rich phase particles is obviously lower than that in the main phase grains, which indicates that Dy is more likely to replace NdPr in the main phase grains, thereby improving the magnetocrystalline anisotropy (H_a) of diffused magnets. But the effect of this method on improving H_{cj} is obviously lower than that of grain boundary diffusion forming a Dy-rich shell layer, which reduces the utilization efficiency of Dy [4].

According to Fig. 4 and Table 1, we speculate that Dy diffusion first enters the Nd-rich phase, and then reaches the grain epitaxial layer, forming a Dy-rich shell layer because of the higher diffusion rate of Dy from the Nd-rich liquid phase into the main phase grains than that inside the main phase grain. After that, grain boundary diffusion and lattice diffusion coexist. As the Dy content in the Nd-rich phase decreases, grain boundary diffusion weakens, and lattice diffusion strengthens. The schematic diagram of Dy diffusion in sintered Nd-Dy-Fe-B magnets is shown in Fig. 5. As the Dy content in the matrix

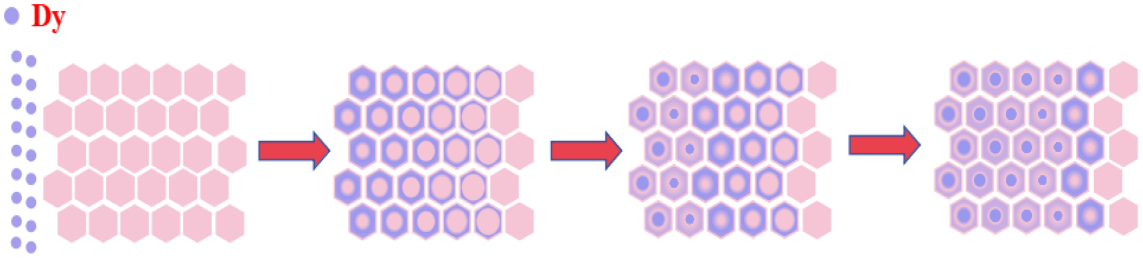

Fig. 5. (Color online) Schematic diagram of Dy diffusion in sintered Nd-Dy-Fe-B magnets.

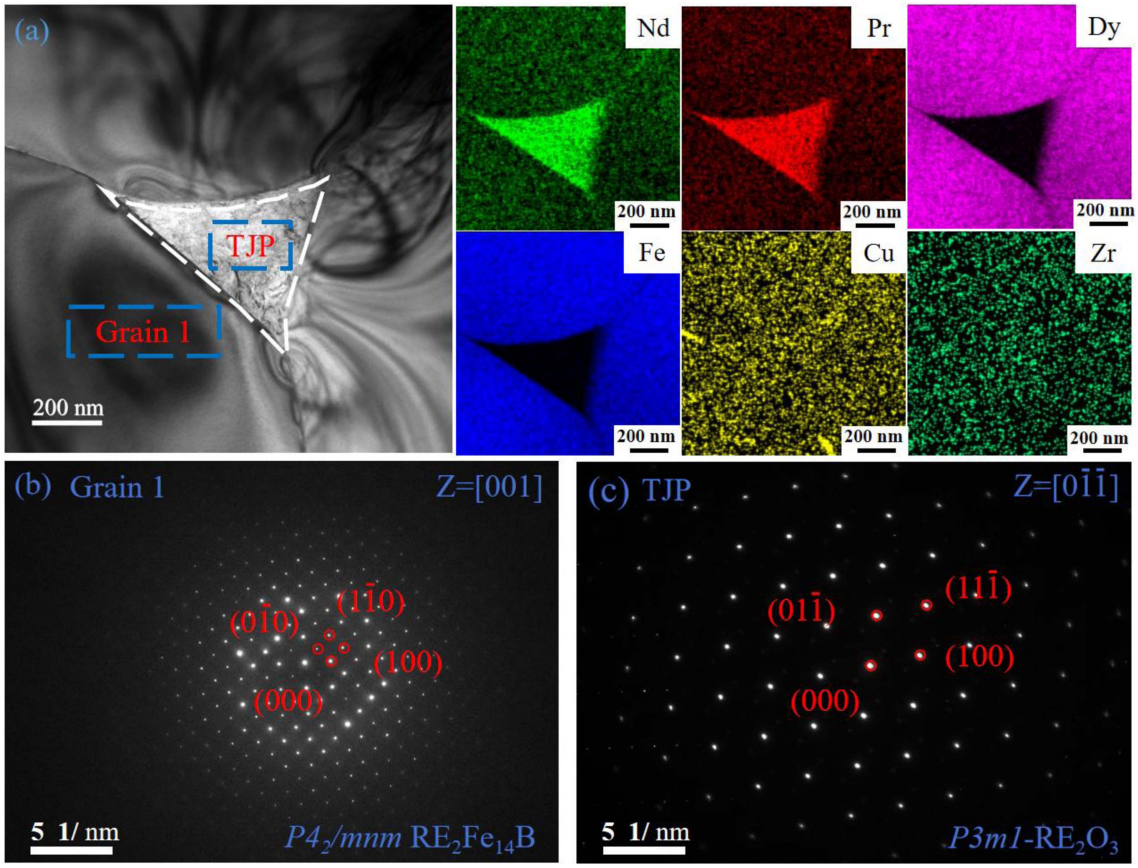

Fig. 6. (Color online) TEM observation and element mapping of the Dy2 matrix. (a) Bright field TEM image and the elemental distribution mappings, (b) SAED pattern of Grain 1 and (c) SAED pattern of TJP.

increases, the diffusion rate of Dy also increases [37]. So, two types of main-phase grain-shell structures begin to appear as the Dy content in the matrix increases from 0 to 1 wt %.

Fig. 6(a) shows the bright-field image and corresponding elemental distribution of the Dy2 matrix, which contains main-phase grains and a small Nd-rich phase particle (TJP). The surface area of the small Nd-rich phase particle is about 0.118 μm^2, which is far smaller than the Nd-rich phase particles used for EDS detection in Fig. 4. Nd and Pr elements are significantly concentrated in the TJP region. In contrast, Dy and Fe elements are enriched in the main phase grains. Cu element enrichment is detected in the TJP region and grain boundaries, which may be the main reason why Cu element can improve the fracture toughness of sintered Nd-Fe-B magnets. The selected-area electron diffraction (SAED) pattern of Fig. 6(b) indicates that the main phase grain (Grain 1) exhibits a 2:14:1 tetragonal structure (space group P42/mnm), with the crystallographic axis aligned along [001]. Fig. 6(c) shows that TJP is the RE_2O_3 phase ($P\bar{3}m1$) in the SEAD pattern, with zone axis [$0\bar{1}\,\bar{1}$]. The hexagonal RE_2O_3 phase is an intermediate phase that acts as an obstacle to Dy atoms rather than forming effective diffusion channels [38].

Fig. 7(A) shows the bright-field image and corresponding elemental distribution of the Dy2 diffused magnet, in which the region contains main-phase grains and a small Nd-rich phase particle (TJP). The surface area of the triple junction phase (TJP) is about 0.304 μm^2, which is larger than that of the RE-rich phase particle in Fig. 6(a). The triple junction phase region includes the Nd_2O_3 phase region (TJP2), the amorphous region (TJP1) and the Zr-rich phase region (RE-Zr). The selected-area electron diffraction (SAED) pattern of Fig. 7(B) indicates that the RE-rich phase (TJP1) belongs to the amorphous phase, and the surface area of the amorphous region is about 0.108 μm^2. The Cu element is detected to be enriched at the TJP1 area, and the Cu content is higher than that of the other two regions, which indicates that the Cu element can promote the formation of the Nd-rich amorphous phase. Fig. 7(C) illustrates the amorphous transition layer and the RE_2O_3 phase ($Ia\bar{3}$) with a zone axis of [$\bar{2}\,\bar{1}\,\bar{1}$] in TJP2. Compared with the hexagonal RE_2O_3 phase ($P\bar{3}m1$) in the matrix detected, the lattice mismatch between c-RE_2O_3 and the main phase is smaller, resulting in higher H_{cj}. The Zr-rich phase region (RE-Zr) shown in Fig. 7(A) is strip-shaped with a surface area of approxi-

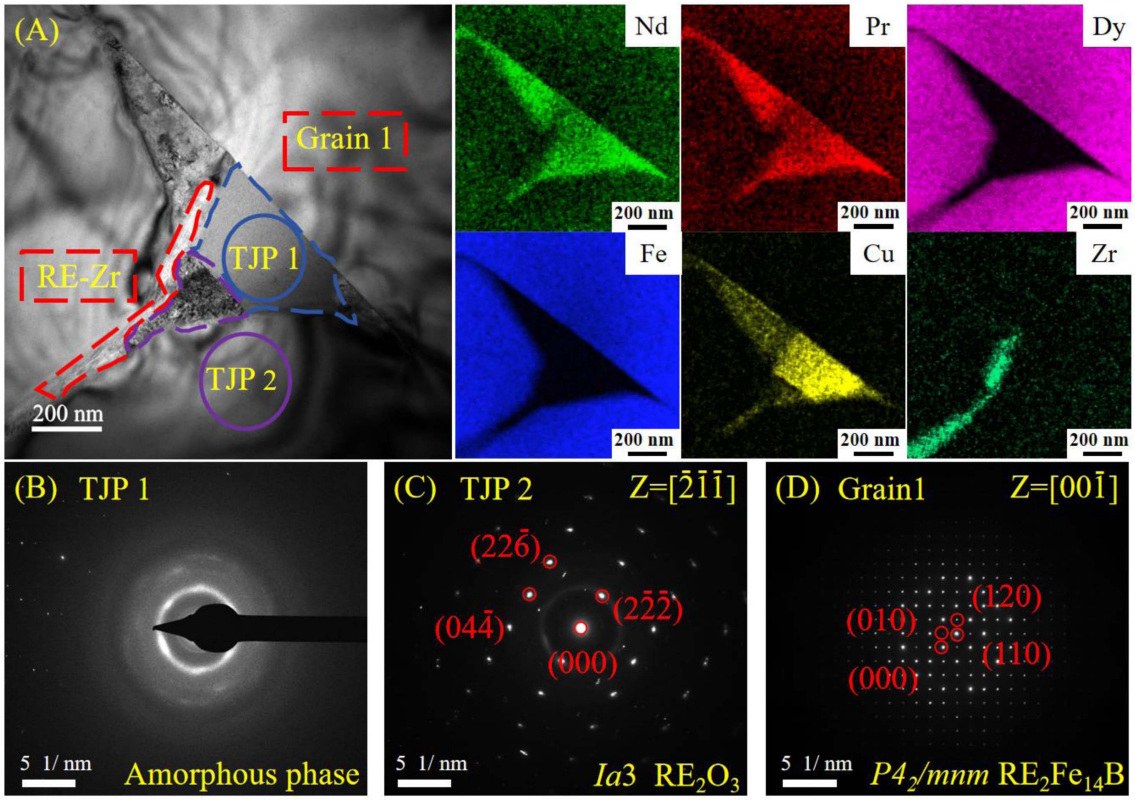

Fig. 7. (Color online) TEM observation and element mapping of the Dy2 diffused magnet: (A) The bright field TEM image and elemental distribution mappings, (B) SAED pattern of TJP1, (C) SAED pattern of TJP2 and (D) SAED pattern of Grain 1.

mately 0.048 μm^2, which is not conducive to the diffusion of the Dy element. The selected-area electron diffraction (SAED) pattern in Fig. 7(D) indicates that the spatial structure of the main phase grain (grain 1) is the same as that in Fig. 6(b).

The grain boundary in Fig. 8(a) is not continuous and uneven, with widths ranging from a few nanometers to over ten nanometers. There exists a continuous grain boundary and the phenomenon of direct contact between grains in Fig. 8(b). Fig. 8(A) and (B) exhibit continuous and smooth lamellar grain boundaries with marked grain boundary widths of 4.5 nm and 6.7 nm, respectively. The Nd-rich phase at grain boundaries thinner than about 2 nm is amorphous and then transforms into a face-centered cubic structure with increasing grain boundary thickness [39]. The spacing of the lattice fringes for the grain boundary between grain 1 and grain 2 is 0.32 nm, corresponding closely to the {111} spacing of the face-centered-cubic (fcc) Nd-rich phase. The spacing of lattice fringes for grain 1 and grain 2 is 0.48 nm and 0.8 nm, respectively.

Meanwhile, the spacing of the lattice fringes at the direct contact between grain 3 and grain 4 is 0.21 nm, and the spacing of the lattice fringes for grain 3 and grain 4 is 0.48 nm and 0.6 nm, respectively. The clear and smooth interface between grains and grain boundaries in Fig. 8 (A) and (B) indicates a minimal lattice distortion near the $RE_2Fe_{14}B/REO_x$ interface. The SEAD pattern of thin Nd-rich phase can be indexed by the fcc structure, which contributes to minimizing phase boundary energy and lattice mismatch to increase the intrinsic coercivity of sintered Nd-Fe-B magnets [40-42].

The Vickers hardness and fracture toughness of matrices and corresponding diffused magnets are shown in Fig. 9. The Vickers hardness of matrices declines slightly, and then increases with increasing Dy content in the matrix. So, Dy addition to the $(NdPrDy)_2Fe_{14}B$ main phase can improve the Vickers hardness of matrices. The Vickers hardness of corresponding diffused magnets increases slightly, and then declines with increasing Dy content in the matrix, indicating that the trend of Vickers hardness with increasing Dy content is opposite to that of the matrix. The Vickers hardness of diffused magnets is higher than that of the matrix when the Dy content in the matrix increases from 0 wt % to 2 wt %, indicating that Dy grain boundary diffusion can increase the Vickers hardness of sintered Nd-Dy-Fe-B magnets. However, the increasing effect of Dy grain boundary diffusion weakens with the increase of Dy content in the matrix. The Vickers

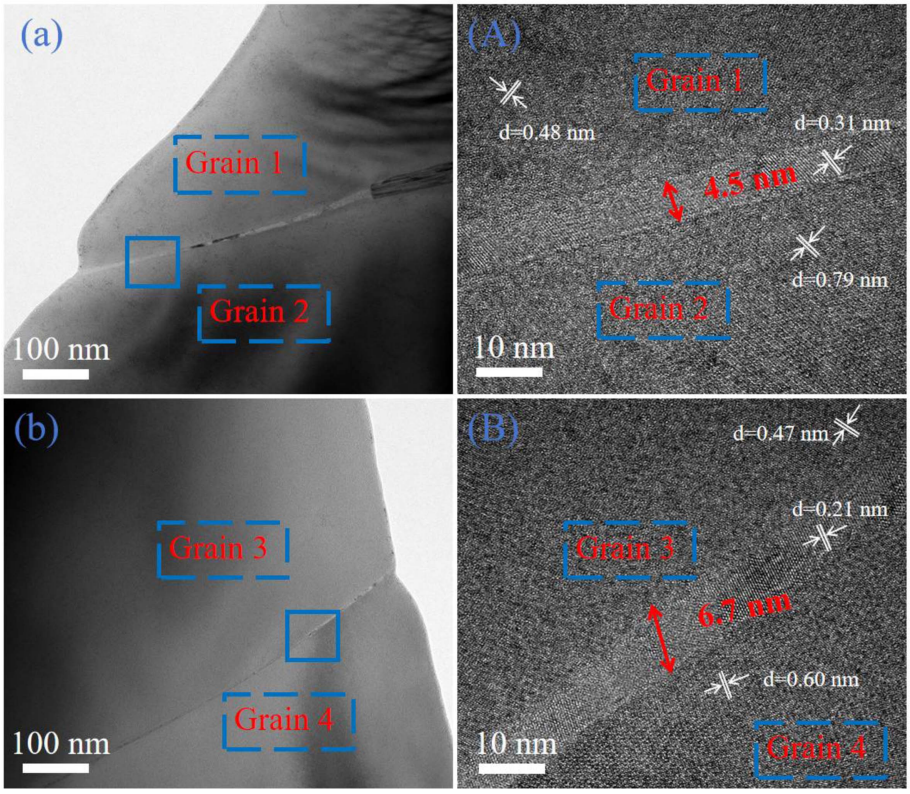

Fig. 8. (Color online) a and b bright field TEM images of the Dy2 matrix and corresponding diffused magnet, (A) and (B) high-resolution TEM images of corresponding GB positions (blue box marking).

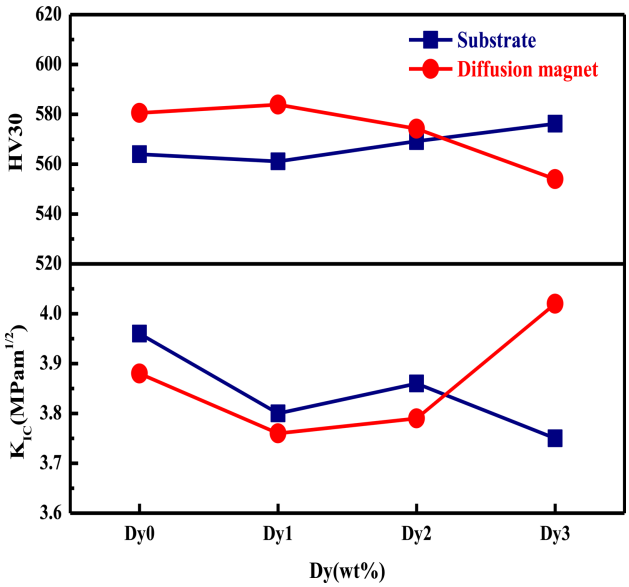

Fig. 9. (Color online) Vickers hardness and fracture toughness of matrices and corresponding diffused magnets.

hardness of diffused magnets is lower than that of the matrix when the Dy content in the matrix increases from 2 wt % to 3 wt %, indicating that Dy grain boundary diffusion reduces the Vickers hardness of diffused magnets. The fracture toughness of diffused magnets declines, then increases with increasing Dy content. The fracture toughness of diffused magnets is lower than that of the matrix when the Dy content in the matrix increases from 0 wt % to 2 wt %, indicating that Dy grain boundary diffusion reduces the fracture toughness of sintered Nd-Dy-Fe-B magnets. However, the fracture toughness of diffused magnets is higher than that of the matrix when the Dy content in the matrix increases from 2 wt % to 3 wt %.

Fig. 10(a) and (A) show BSE SEM images of the Dy3 matrix and the corresponding diffused magnet. It can be seen that there are many obvious defects on the surface of the diffused magnet after Dy grain boundary diffusion, which reduces the uniformity of microstructure and internal composition of the diffused magnet, and increases the possibility of generating demagnetization domains in the first quadrant, leading to a significant decrease in the B_r of the diffused magnet. Overall, the Nd-rich phase content increases, the white particle distribution becomes more dispersed and uniform, and the size of white Nd-rich phase particles decreases after Dy grain boundary diffusion. The Vickers hardness of the grain boundary Nd-rich phase is only 262 HV, significantly lower than that (900HV) of the main phase [43]. The primary fracture mechanism of sintered Nd-Fe-B magnets is intergranular fracture, and the white Nd-rich phase particles can effectively inhibit crack expansion, thereby improving the fracture toughness of sintered Nd-Fe-B magnets [18]. So the occurrence of the above phenomena reduces the Vickers hardness of the diffused magnet and increases its fracture toughness. Fig. 10(b) and (B) show secondary electron images of the Dy3 matrix and corresponding diffused magnet. The grain boundaries of the two samples are unclear and discontinuous, and there is also partial direct contact between grains, which is beneficial for improving the fracture toughness of magnets. The average grain size of diffused magnets is larger than that of the matrix, as shown in Fig. 10(d) and (D). The increase in grain size reduces the total area of the grain boundary, increases the resistance to crack propagation, and thus

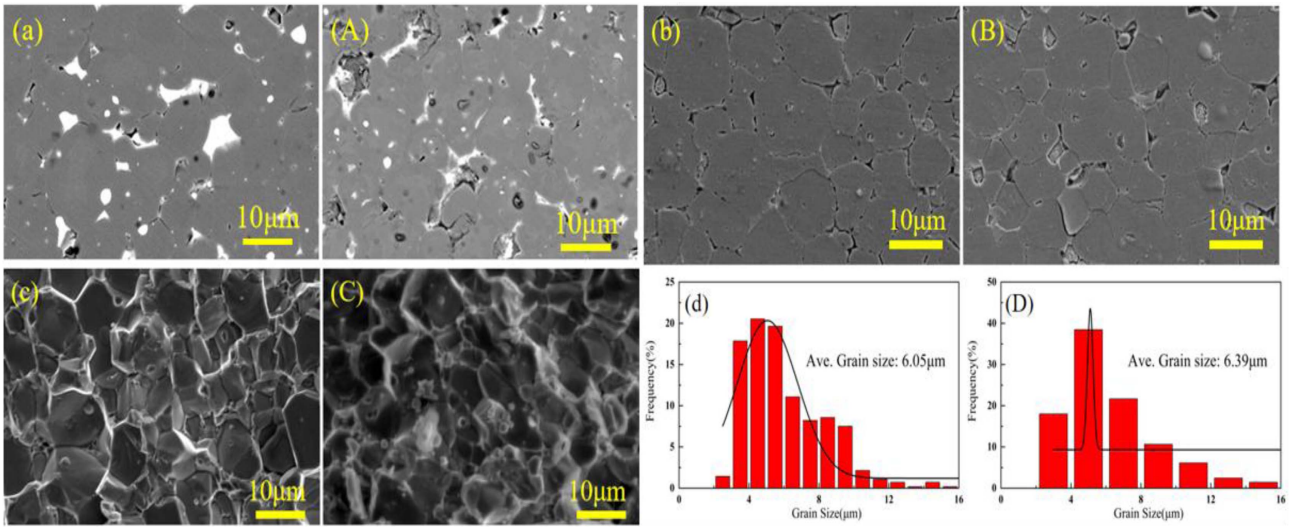

Fig. 10. (Color online) SEM images and grain size statistics of the Dy3 matrix (a-d) and corresponding diffused magnet (A-D).

improves the fracture toughness of the diffused magnet. There exist a few transgranular fracture grains in Fig. 10 (c) and (C), and the number of Nd-rich phase particles on the fracture surface of the diffused magnet is significantly higher than that of the matrix. There is a noticeable tearing phenomenon at the fracture crystal interface, which is obviously different from the typical intergranular rock sugar morphology. Therefore, the fracture toughness of the diffused magnet significantly increases when the Dy content of the matrix is 3 wt %.

4. Conclusions

Dy addition and Dy grain boundary diffusion can increase the H_{cj} of sintered Nd-Fe-B magnets, resulting in a higher H_{cj} of corresponding diffused magnets than the matrix. The fracture toughness of matrices declines overall with increasing Dy content. Still, it is higher than that of corresponding diffused magnets when the Dy content in the matrix increases from 0 wt % to 2 wt %. The Dy-rich shell of $(Dy, Nd)_2Fe_{14}B$ phase is observed after diffusion of the Dy0 matrix, and a large number of core-shell structure (Dy-rich core and Dy-lean shell) grains are found with increasing Dy coating content. The Al element is detected in both the main phase grains and the white Nd-rich phase particles, while Cu and Zr elements only exist in the white Nd-rich phase particles. The hexagonal RE_2O_3 phase ($P\bar{3}m1$) and the cubic RE_2O_3 phase ($Ia\bar{3}$) are detected in TJP, and there exists the triple junction phase consisting of the Nd_2O_3 phase, the amorphous phase and the Zr-rich phase.

Acknowledgments

This work was supported by the Hubei Provincial Natural Science Joint Fund Project (2025AFD189) and the Innovation and Entrepreneurship Training Project for College Students (DC2024021).

References

[1] O. Gutfleisch, M. A. Willard, E. Brück, C. H. Chen, S. G. Sankar, and J. P. Liu, Adv. Mater. **23**, 821 (2011).
[2] H. Nakamura, Scr. Mater. **154**, 273 (2018).
[3] F. Chen, J. Magn. Magn. Mater. **514**, 167227 (2020).
[4] Z. W. Liu, J. Y. He, and R. V. Ramanujan, Mater. Des. **209**, 110004 (2021).
[5] M. Lv, T. Kong, W. H. Zhang, M. Y. Zhu, H. M. Jin, W. X. Li, and Y. Li, J. Magn. Magn. Mater. **517**, 167278 (2021).
[6] M. Ji, Z. J. Wang, W. Q. Liu, Y. Q. Li, H. Chen, H. H. Wu, R. H. Du, D. T. Zhang, M. Yue, X. F. Yi, Y. H. Liu, and S. S. Zha, J. Alloys. Compd. **970**, 172598 (2024).
[7] L. Zhou, J. Li, X. H. Cheng, T. Liu, X. J. Yu, and B. Li, J. Rare. Earths. **35**, 559 (2017).
[8] H. H. Wu, Y. Q. Li, W. Q. Liu, Z. J. Wang, Y. Qin, M. Ji, R. H. Du, D. T. Zhang, L. L. Zhang, M. Yue, X. F. Yi, Y. H. Liu, and S. S. Zha, Mater. Charact. **210**, 113817 (2024).
[9] Z. Wang, T. T. Sasaki, Y. Une, T. Ohkubo, and K. Hono, Acta. Mater. **248**, 118774 (2023).
[10] W. Q. Liu, Y. Li, D. Wu, M. Yue, Z. J. Wang, S. S. Zha, Y. H. Liu, X. F. Yi, and Y. H. Du, J. Rare. Earths. **39**, 682 (2021).
[11] T. H. Kim, S. R. Lee, S. J. Yun, S. H. Lim, H. J. Kim, M. W. Lee, and T. S. Jang, Acta. Mater. **112**, 59 (2016).
[12] W. Tang, K. W. Dennis, M. J. Kramer, I. E. Anderson, and R. W. McCallum, J. Appl. Phys. **111**, 07A736 (2012).
[13] K. H. Bae, T. H. Kim, S. R. Lee, H. J. Kim, M. W. Lee, and T. S. Jang, J. Alloys. Compd. **612**, 183 (2014).
[14] J. H. Yan, Q. Wu, X. K. Hu, J. G. Jia, Y. Zhao, M. Zou, and H. L. Ge, J. Magn. Magn. Mater. **600**, 172129 (2024).
[15] A. S. Kim, Phys. **63**, 3519 (1988).
[16] S. H. Liang, X. H. Shao, Y. S. Que, B. Guo, H. P. Bao, G. C. Tang, X. L. Yan, J. S. Bao, L. J. Yang, L. S. Qin, K. Y. Shu, D. Chen, and Z. L. Song, J. Alloys. Compd. **1003**, 175689 (2024).
[17] C. Luo, X. M. Qiu, H. M. Wang, and F. Xing, J. Manuf. Process. **64**, 323 (2021).
[18] W. Li, A. H. Li, H. J. Wang, W. Pan, and W. H. Chang, J. Appl. Phys. **105**, 07A703 (2009).
[19] H. J. Wang, A. H. Li, and W. Li, Intermetallics **15**, 985 (2007).
[20] L. N. Zhao, X. L. Wang, K. H. Ding, S. L. Cui, Y. C. Sun, and M. S. Li, Rare Met. **41**, 2688 (2022).
[21] Z. H. Hu, D. W. Ma, H. J. Qu, J. Q. Zhao, C. Luo, and H. J. Wang, IEEE. Trans. Magn. **51**, 1 (2015).
[22] Z. H. Hu, L. H. Chu, J. Li, and Y. Liu, J. Magn. Magn. Mater. **324**, 101 (2012).
[23] S. Hirosawa, Y. Matsuura, H. Yamamoto, S. Fujimura, M. Sagawa, and H. Yamachi, J. Appl. Phys. **59**, 873 (1986).
[24] S. Z. Zhou and Q. F. Dong, Super Strong Permanent Magnet - Rare Earth Iron based Permanent Magnet Materials, 2nd edn, Metallurgical Press (1999) pp. 251.
[25] S. Sugimoto, J. Phys. D. Appl. Phys. **44**, 064001 (2011).
[26] K. Hono and H. Sepehri-Amin, Scr. Mater. **151**, 6 (2018).
[27] M. Soderznik, H. Sepehri-Amin, T. T. Sasaki, T. Ohkubo, Y. Takada, T. Sato, Y. Kaneko, A. Kato, T. Schrefl, and K. Hono, Acta. Mater. **135**, 68 (2017).
[28] Y. Qin, Y. Q. Li, Z. J. Wang, H. H. Wu, L. L. Zhang, W. Q. Liu, and M. Yue, J. Mater. Res. Technol. **29**, 1805 (2024).
[29] B. A. Cook, J. L. Harringa, F. C. Laabs, K. W. Dennis, A. M. Russell, and R. W. McCallum, J. Magn. Magn. Mater. **233**, L136 (2001).
[30] C. Qin, S. S. Zheng, X. F. Liao, X. Wang, W. W. Zeng, Q. Y. Lu, D. Y. Chen, S. N. Xu, Z. W. Liu, and Q. Zhou, J. Mater. Res. Technol. **35**, 3556 (2025).

[31] Z. H. Zhang, H. S. Chen, J. Y. Jin, B. Y. Lim, X. L. Liu, W. Li, M. Yan, and S. P. Ringer, Acta. Mater. **261**, 119344 (2023).
[32] J. Fidler, K. G. Knoch, H. Kronmüller, and G. Schneider, J. Mater. Res. **4**, 806 (1989).
[33] B. Grieb, K. G. Knoch, E. T. Henig, and G. Petzow, J. Magn. Magn. Mater. **80**, 75 (1989).
[34] A. S. Kim and F. E. Camp, J. Appl. Phys. **79**, 5035 (1996).
[35] S. Pandian, V. Chandrasekaran, G. Markandeyulu, K. J. L. Iyer, and K. V. S. Rama Rao, J. Appl. Phys. **92**, 6082 (2002).
[36] W. Z. Su, J. H. Lu, L. Xiao, G. Fu, D. W. Shi, C. Wang, Z. Y. Yu, and P. Wu, Mater. Charact. **224**, 115016 (2025).
[37] K. Loewe, D. Benke, C. Kübel, T. Lienig, K. P. Skokov, and O. Gutfleisch, Acta. Mater. **124**, 421 (2017).
[38] T. H. Kim, S. R. Lee, H. J. Kim, M. W. Lee, and T. S. Jang, Acta. Mater. **93**, 95 (2015).
[39] Y. Shinba, T. J. Konno, K. Ishikawa, K. Hiraga, and M. Sagawa, J. Appl. Phys. **97**, 053504 (2005).
[40] Q. Z. Liu, J. Xu Wang, X. P. Dong, L. T. Zhang, and J. Y. Yang, Scr. Mater. **68**, 687 (2013).
[41] K. Makita and O. Yamashita, Appl. Phys. Lett. 74, 2056 (1999).
[42] R. S. Lai, Q. Ma, H. B. Xu, Y. Y. Zhang, Z. B. Li, and B. G. Shen, Rare. Met. **44**, 2629 (2025).
[43] Y. M. Rabinovich, V. V. Sergeev, A. D. Maystrenko, V. Kulakovsky, S. Szymura, and H. Bala, Intermetallics **4**, 641 (1996).